Journal of Aerosol Science 107 (2017) 14–30

Contents lists available at ScienceDirect

Journal of Aerosol Science

journal homepage: www.elsevier.com/locate/jaerosci

Scavenging of micron-scale particles using a combination of fog and a cylindrical ultrasonic standing wave field

T. Merrell, J.R. Saylor*

Clemson University, Department of Mechanical Engineering, Clemson, SC 29634, USA

ARTICLE INFO

Keywords:
Particles
Fog
Scavenging
Ultrasonics

ABSTRACT

An experimental study is presented wherein a cylindrical ultrasonic standing wave field is used to increase the scavenging of micron-scale particles by water fog in an air stream. The cylindrical standing wave field was generated with a cylindrical resonator composed of a metal tube driven by three ultrasonic transducers. The nodes in the resonator took the form of concentric cylinders extending the length of the tube. Experiments conducted with the resonator yielded maximum scavenging coefficients over four times that obtained previously with a disk shaped geometry. The effect of both air flow rate and input power are investigated, and insights are presented on the mechanism of particle removal by drops in the presence of a standing wave field.

1. Introduction

It is estimated that the United States produces 8000 Mg/year of fine particulate matter pollution, defined as particles less than 2.5 μm in diameter ($PM_{2.5}$), a significant portion coming from the burning of fossil fuels (Tucker, 2000). If inhaled, $PM_{2.5}$ can have particularly deleterious effects on the pulmonary health of humans (Cohen, 2000; Fann et al., 2012; Johnson, 2004; Seaton, MacNee, Donaldson, & Godden, 1995;). This is because inhaled $PM_{2.5}$ can penetrate deep into the lungs where it has a particularly high deposition rate (Heyder, Gebhart, Rudolf, Schiller, & Stahlhofen, 1986). The health effects caused by exposure to $PM_{2.5}$ can lead to death, as studies have shown that mortality rates correlate to local $PM_{2.5}$ concentration in the atmosphere (Pope et al., 1995; Schwartz, Laden, & Zanobetti, 2002). Traditional methods for removing particles, such as wet scrubbers, electrostatic precipitators, and baghouses, generally do well over a large range of particle diameters, but perform poorly at particle diameters on the order of a micron (Kim, Jung, Oh, & Lee, 2001; Kim & Lee, 1999; Lee & Liu, 1980). As such, improvements are needed to increase the collection efficiency of micron-scale particles.

A commonly used technology for removal of particulate pollutants from exhaust streams is the wet scrubber which has several advantages, including robustness, an ability to work on particles regardless of their chemical composition, and an ability to also remove gases. However, like many particle removal technologies, wet scrubbers perform poorly on particles having an effective diameter on the order of a micron. In an effort to improve upon the effectiveness of the wet scrubber, researchers have studied the use of acoustic waves to enhance particle-drop interactions in such devices. Ran, Saylor, and Holt (2014) and Ran and Saylor (2015) demonstrated the ability to scavenge micron-scale particles from an air stream using a combination of an ultrasonic standing wave field and water drops. These researchers used a disk shaped transducer to excite an ultrasonic standing wave field in which particles and water drops combined in the nodes of the field, as shown in Fig. 1. As particles and drops combined they grew into much larger particle-laden drops which eventually fell from the system, thus removing particles in the process. The practical application of the above approach was limited by modest particle collection and relatively low air flow rates. For example, the maximum particle

* Corresponding author.
E-mail addresses: jsaylor@clemson.edu (J.R. Saylor).

http://dx.doi.org/10.1016/j.jaerosci.2017.01.001
Received 15 July 2016; Received in revised form 11 December 2016; Accepted 3 January 2017
Available online 09 January 2017

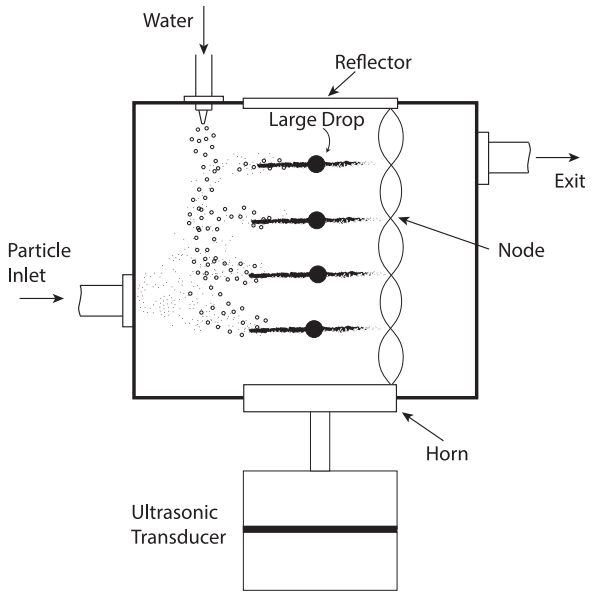

Fig. 1. Illustration of the setup used by Ran et al. (2014) to remove micron sized particles from an air flow.

collection reported by the authors was ~20% at an air flow rate of 12 L/min. Increasing both the percentage of particles collected and the air flow rate would facilitate practical application of the described approach in wet scrubbers. This need for an increase in particle removal and operating air flow rate is an important motivation for the present study.

A major constraint of the setup used in Ran et al. (2014) and Ran and Saylor (2015) was the relatively short residence time for particles and drops as they traveled through the ultrasonic standing wave field, which is roughly equal to the diameter of the disk-shaped transducer divided by the flow velocity. Scavenging of particles would be increased by increasing the residence time, however doing so requires either a reduction in the flow rate, which is not desired, or an increase in the size of the disk-shaped transducer. Commercially available disk-shaped ultrasonic transducers are currently limited to diameters on the order of an inch, leaving little room for improvement on this disk-shaped transducer approach.

An alternative approach to the work of Ran et al. (2014) and Ran and Saylor (2015) would be to use a cylindrical geometry like that shown in Fig. 2. If such a cylinder could be excited to oscillate in the breathing mode (axially symmetric expansion and contraction of the tube diameter), forming a cylindrical resonator, then an ultrasonic standing wave field could be created within the cylinder where the nodes would take the form of concentric cylinders extending the length of the cylinder. In such a geometry the residence time for a given flow rate could be increased simply by making the tube longer and would therefore be essentially unlimited (of course the acoustic power delivered to the standing wave field would still be limited to the total power delivered to the cylindrical resonator). An increased residence time would allow more time for drops and particles to combine in the nodes. Furthermore, even if the cylindrical resonator shown in Fig. 2 were modest in length, as long as most of the particles and drops had migrated to the nodal regions at the resonator exit, these regions of high particle/drop concentration could be maintained if a passive tube was connected to the cylinder exit. The passive tube concept is shown in Fig. 3. Thus, once particles and drops are moved by the acoustic radiation force to nodes, they should then remain in approximately the same radial location, allowing more time for particle/drop combinations to occur. The passive tube could potentially be much longer than the cylindrical resonator itself, thus greatly enhancing the overall residence time and subsequently the number of particle/drop combinations. Such a possibility does not exist for the disk setup (Fig. 1), where drops and particles are in close proximity as they flow through the nodes, but the nodal structure of high particle/drop

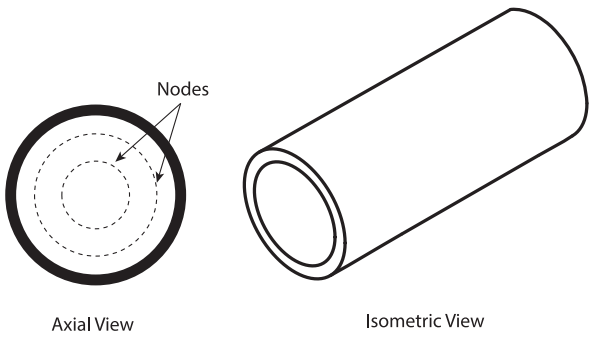

Fig. 2. Schematic of a cylindrical resonator showing the cylindrical nodes that would result should the tube be oscillated in the breathing mode.

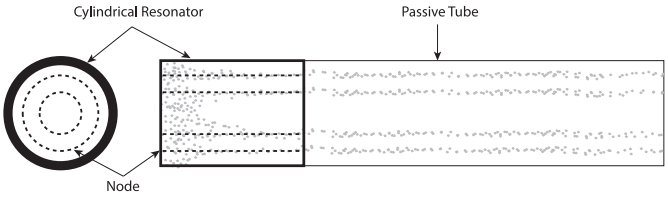

Fig. 3. Depiction of a passive tube connected downstream of a cylindrical resonator, resulting in an increased residence time for the concentrated particle/drop combination.

concentration is lost as the flow leaves the standing wave field and exits the box. An additional benefit of a cylindrical geometry is that the acoustic field is more focused than for the case of the disk shaped transducer. In the case of the cylindrical resonator, the reflector is essentially the axis of the cylinder and, other than the ends of the tube, there is no loss of acoustic energy due to divergence of the field, improving the overall performance.

Finally, the shape of a cylindrical resonator is more favorable than the disk shaped transducer in terms of the fraction of flow that travels through the ultrasonic standing wave field. A disk shaped transducer has an open design, meaning flow through the field needs to be contained by something other than the transducer and reflector. Ran et al. (2014) and Ran and Saylor (2015) forced particles and drops into the standing wave field by enclosing the disk shaped transducer and reflector inside of a box, but even in such a configuration, not all of the flow passed through the acoustically active region. A cylinder, on the other hand, would act as both a resonator and a pipe to contain and direct the flow. Fig. 4 shows a depiction of the difference in flow containment for a disk versus a cylinder. As shown, the flow is guaranteed to go through the acoustically active region for the cylindrical case, while a portion of it misses the acoustically active region for the disk geometry.

One method for implementing a cylindrical geometry would be to use a cylinder composed of piezo material. Such an approach was taken by Kaduchak, Sinha, and Lizon (2002) and Yang, Hwang, Youngmin, and Moojoon (2012), who both demonstrated the ability to establish a cylindrical standing wave field inside a cylinder made of PZT (lead zirconate titanate). However, as is the case of PZT disk transducers, significant restrictions exist on the size of commercially available PZT cylinders, which would obviate the very benefits of variable size cylinders described above. Accordingly a different approach was taken herein as is described in the next section.

Summarizing, an ultrasonic standing wave field has been shown to enhance scavenging of micron-scale particles by drops. However, the disk shaped geometry that has been used has drawbacks which a cylindrical geometry may alleviate. The goal of the present work is to determine if the cylindrical geometry will indeed perform better, and to determine the scavenging capability of a cylindrical resonator as a function of power and flow rate.

2. Methods

The cylindrical resonator used herein is shown in Fig. 5. The resonator was a hollow aluminum cylinder excited by three bolt clamped Langevin transducers. The transducers were spaced around the cylinder in 120° increments and were located in the mid-plane of the cylinder. In order to excite a standing wave field inside the aluminum cylinder, it was necessary that the transducers be driven at their natural frequency and that the driving frequency match a breathing mode resonance for the air cavity and a natural frequency for the tube itself. Due to the density of resonant frequencies that exist for a cylinder, adequate frequency matching was

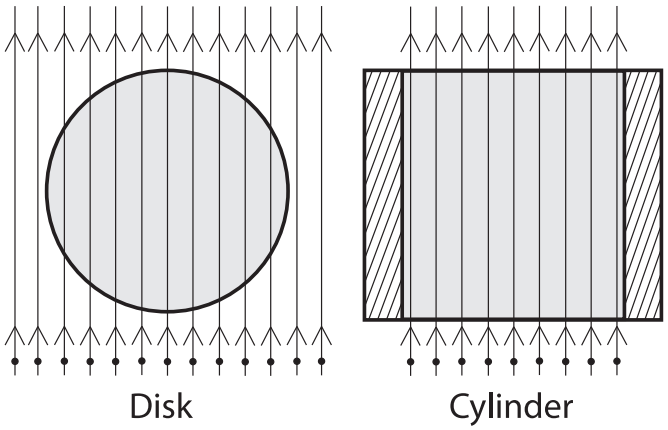

Fig. 4. Flow containment comparison for disk and cylinder where the gray regions are the acoustically active areas. In the disk case, a portion of the flow misses the acoustically active region, while for the cylindrical case all of the flow goes through the acoustically active region.

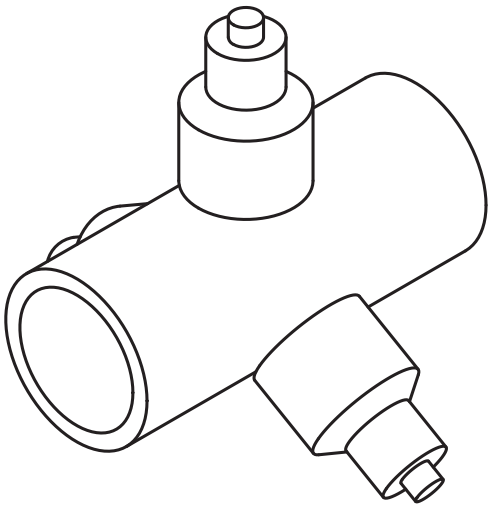

Fig. 5. Cylindrical resonator showing the three Langevin transducers used to drive it.

easily achieved. The cylinder used herein had an inner diameter of 5.08 cm, an outer diameter of 6.35 cm, and a length of 12.7 cm. The natural frequency of the Langevin transducers was 28 kHz, and the resonance frequencies closest to this for the air cavity and the aluminum cylinder were 28.35 kHz and 28.04 kHz, respectively. When driven together the entire system found resonance at a slightly higher frequency of 29.3 kHz. This actual resonant frequency was found experimentally by monitoring the power delivered to the entire setup and identifying the frequency at which peak power was consumed for a constant voltage delivered to the transducers. The discrepancy between the predicted and actual resonant frequency is not surprising given the complicated two-way coupling between the transducers, the air cavity, and the cylinder. For example, the resonance of the tube itself is based on vibration theory for a simple tube, while in fact the tube has three transducers mounted upon it which adds significant mass to the tube and which is not accounted for in the theory.

Fig. 6 is a schematic illustration of the experimental setup. Particle scavenging was quantified by the scavenging coefficient defined as:

$$E = \frac{W_u - W_d}{W_u} \tag{1}$$

where W is the particle number density measured by the particle counters (MetOne, Hach Ultra Analytics), and the subscripts u and d represent the upstream and downstream locations, respectively. The first (upstream) particle counter was located right before the fog generator (described below), and is labeled Particle Counter #1 in Fig. 6. The second (downstream) particle counter was located at the exit of the test section and is labeled Particle Counter #2 in Fig. 6. Values of E were obtained both with and without ultrasonics to determine the degree of improvement due to ultrasonics. There was no change in the experimental setup for the measurements without ultrasonics; the power to the transducers was simply turned off. Because measurements of W must not include drops, diffusion dryers were installed before the downstream particle counter to ensure that drops were not counted. As described later, steps were taken to account for particle deposition in the diffusion dryers as well as in other parts of the apparatus.

The particles used here were smoke obtained from an incense stick which was injected into the system with a syringe pump. These particles were chosen for two reasons. First, generation of particles by simply burning an incense stick was inexpensive and straightforward. Each run simply required lighting and then quickly extinguishing an incense stick inside of the syringe. Second, the smoke produced from the incense stick had a large number of particles on the order of a micron, the diameter of interest for the current work. The ratio of clean air to particle laden air from the syringe pump was about 10,000:1. This flow rate ratio was actually varied somewhat to ensure a relatively constant particle number density as the air flow rate was changed, as is described below. It was always the case that the additional flow from the syringe pump was negligible compared to the air flow rate.

To ensure that the particle counters were equally sensitive, the setup shown in Fig. 7 was used to check for measurement similarity. By ensuring that tube lengths leading up to the individual particle counters were equal, any differences between the two counters was a measure of error. Experiments with the Fig. 7 setup revealed <1% difference between the average readings of the two particle counters over a 9 minute interval, which was the duration of a scavenging run.

A typical particle size distribution of the incense smoke as measured by one of the particle counters is shown in Fig. 8, where d_P is the particle diameter. Only the first four bins of the particle counters were populated by more than one particle on any given run, as is the case in Fig. 8. More details of the particle distribution are presented in Table 1 which provides the average particle number density in number per cubic centimeter (#/cc) as well as the standard deviation, for each bin. These average and standard deviation values are given for each air flow rate explored. As was noted earlier, the syringe pump flow rate was manually varied in an attempt to maintain a constant particle number density, regardless of flow rate. In spite of this, small variations in particle number density were observed, as Table 1 shows. Focusing on bin one, which is the most populated bin, the particle number density decreases by 38%

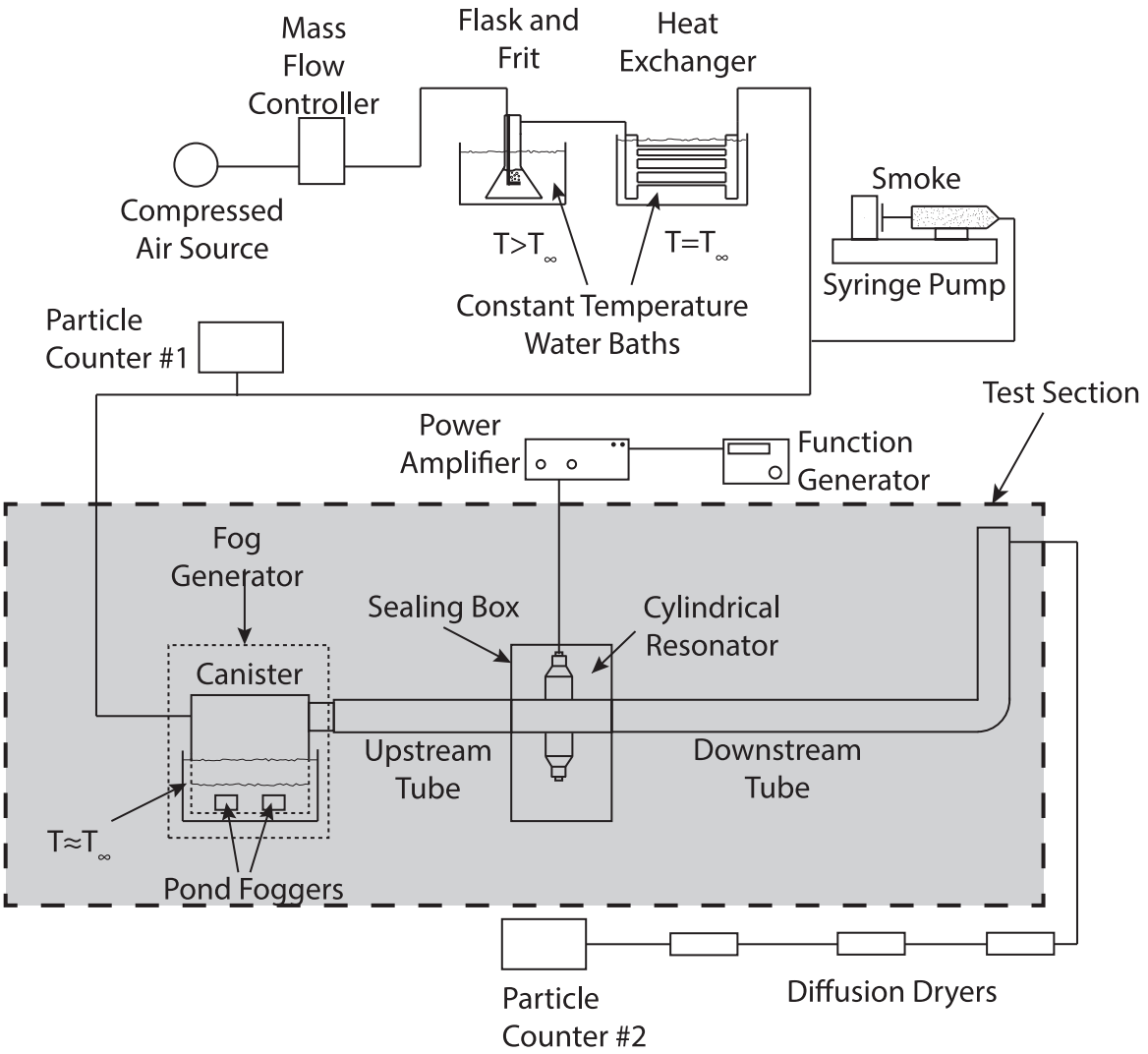

Fig. 6. Schematic of experimental setup used for particle scavenging. The gray area is the test section where actual particle scavenging occurred.

over the range of air flows explored, which is reasonable considering that the flow rate was varied by a factor of 3.5. Considering the first bin again, averaged over all of the flow rates considered, the ratio of the standard deviation to the average number density was 20%.

Fog was generated with pond foggers (Alpine, FG100) inside an airtight canister filled with doubly distilled water. The pond foggers were themselves ultrasonic transducers, operating at a frequency of 1.7 ± 0.04 MHz and directed upward at the water surface from below. The interaction of the acoustic waves with the water surface resulted in the formation of a large number of small fog drops. Measures were taken to ensure that the water level in the canister was the same at the beginning of each run; it was 6 cm from the bottom of the canister. The drop size distribution (DSD) of the fog drops is presented in Fig. 9, where d_d is the drop diameter. The DSD was obtained by coating a microscope slide with a small amount of paraffin oil and then holding the slide perpendicular to the flow of air and water drops at the canister exit. Drops were allowed to impact the microscope slide surface for about ten seconds, after

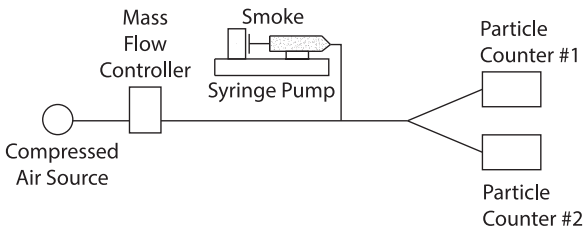

Fig. 7. Schematic of experimental setup used to check agreement between particle counters.

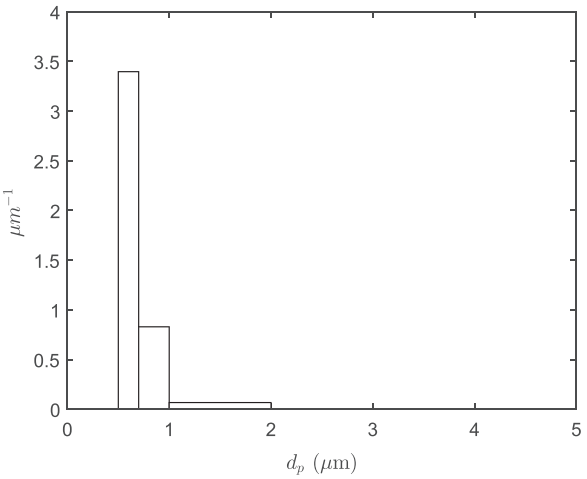

Fig. 8. Particle size distribution for smoke used in the experiments. Results are presented as a fraction of total in a particle bin, scaled to the width of that bin in μm.

which they were imaged using a digital camera (Cannon, EOS Rebel T3) mounted on a microscope (Leica DM750). The conversion factor for the optical system was 0.05 μm/pixel and the Abbe resolution limit was 0.25 μm. A customized macro in ImageJ (Rasband, 2009) software was used to measure the size and number of drops in each image. The sizing and counting was done by first converting the image from grayscale to black and white, after which a particle counting algorithm built into the software was used to count and size the number of circular objects in the image. To obtain the DSD presented in Fig. 9, a total of thirty images were used, yielding approximately 600 drop diameter measurements. In order to ensure an individual drop was not measured multiple times, only 3–4 images were taken from each slide, and the field of view was moved significantly for each image. The measured median diameter was 5.8 μm with an rms of 2.4 μm.

The method for capturing drops on a microscope slide described above is essentially a modified version of an impactor (Marple, Liu, & Whitby, 1974). Impactors are typically described by their cutoff diameter, the diameter at which 50% of the particles are collected for a given nozzle-plate combination. A point of possible concern here is that only drops larger than the cutoff diameter are reported with smaller drops ignored. Predictions of the cutoff diameter are virtually always for setups where the ratio between the

Table 1
Average and standard deviation of the particle number density for each bin and for each air flow rate Q explored. The particle diameter ranges measured in each bin are as follows: Bin 1: 0.5 μm–0.7 μm; Bin 2: 0.7 μm–1.0 μm; Bin 3: 1.0 μm–2.0 μm; Bin 4: 2.0 μm–3.0 μm; Bin 5: 3.0 μm–5.0 μm; Bin 6: >5.0 μm. Bins 5 and 6 were not populated in the experiments presented herein.

Q (L/min)	Bin #	Average concentration (#/cc)	Standard deviation (#/cc)
20	1	30.71	2.062
	2	8.027	2.696
	3	1.608	0.8544
	4	0.1123	0.06348
30	1	25.46	4.598
	2	8.716	3.373
	3	2.036	1.384
	4	0.1256	0.0940
40	1	22.88	4.599
	2	7.878	3.373
	3	1.989	1.358
	4	0.1237	0.9400
50	1	23.14	4.975
	2	8.707	3.397
	3	2.217	1.353
	4	0.1417	0.1048
60	1	21.48	5.974
	2	7.697	3.563
	3	2.152	1.494
	4	0.1408	0.1024
70	1	18.89	4.602
	2	7.167	2.926
	3	1.902	1.139
	4	0.1169	0.07909

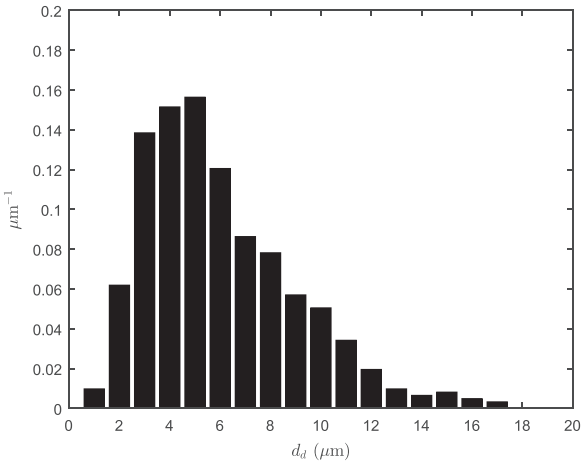

Fig. 9. Drop size distribution for fog water drops.

nozzle-to-plate distance and the nozzle diameter are of order unity (Hinds, 1982; Liu, 1975; Marple & Willeke, 1976), while in this work, the microscope slide was much closer than a nozzle diameter to the nozzle. Hence, existing impactor relationships cannot be used to confirm the value of drop diameters that were obtained here. An alternative approach to confirming the measured fog drops diameters is to note that the foggers used in this work operate by generating Faraday waves (Faraday, 1831) on the surface of the water. When the Faraday wave amplitude is high, drops are ejected from the peaks of the Faraday waves, creating a monodisperse drop size distribution having a diameter of the same order as that of the half wavelength of the Faraday wave (Lang, 1962; McCubbin, 1953; Peskin & Raco, 1963; Wood & Loomis, 1927). As noted earlier, the foggers used here operated at a frequency of 1.7 ± 0.04 MHz. The linear dispersion relationship for waves is (Dietrich, 1963):

$$c^2 = \left[\left(\frac{g\lambda}{2\pi}\right)\left[\frac{(\rho_w - \rho_a)}{\rho_w}\right] + \left[\frac{\sigma}{(\rho_w - \rho_a)}\right]\left(\frac{2\pi}{\lambda}\right)\right]\tanh\left(\frac{2\pi h}{\lambda}\right) \tag{2}$$

where c is the wave phase speed, σ is the surface tension, g is gravitational acceleration, ρ_w is water density, ρ_a is the air density, λ is the wavelength, and h is the water depth. Substituting $c = \lambda f_w$, where f_w is half the frequency of the fogger (since these are Faraday waves) allows for the wavelength to be calculated. Neglecting the gravitational term since at these frequencies the waves will be essentially pure capillary waves, and ignoring the hyperbolic tangent term since at these wavelengths the water layer is essentially infinitely deep, gives a wavelength of 8.6 μm. Since each individual wave will produce a drop only at the peak, the generated drop will be on the order of half the wavelength, which is 4.3 μm. Hence the predicted drop diameter is very close to the measured median value of the fog in the experiment. Of course, details of the drop formation at the wave surface will change the value from the computation presented here, but the expected diameters should still be of the same order.

The liquid flow rate of water drops into the system was measured with a simple conservation of mass method. The mass of the liquid canister was measured before and after each run with a mechanical balance (Ohaus, Triple Pro 2610) having 0.1 g resolution. The liquid flow rate was computed as the decrease in mass divided by the experimental duration. Typical masses measured range from 4 g to 18 g giving resolution errors ranging from 2.5% to 0.5%.

In order to reduce evaporative loss from the fog drops as they traveled through the setup, the air was humidified by first bubbling it through a glass frit in a constant temperature water bath held below room temperature (21 °C–24 °C), as shown in Fig. 6. The humidified air then entered a heat exchanger, consisting of a set of tubes immersed in a separate constant temperature water bath held at room temperature (25 °C). The described process gave the air a relative humidity (RH) of 80% prior to entering the test section. Preliminary experiments conducted at RH ~100% showed anomalous results, most likely due to condensation on particles. Such problems did not occur for RH = 80%. The relative humidity was measured before each run with a hygrometer (DigiSense HumidityLogR) to verify that RH = 80 ± 1% at the entrance of the test section. Despite this humidification of the air sent to the canister inlet, there was still a finite amount of evaporative loss from the drop due to the fact that RH = 80% at the inlet to the canister ($viz < 100\%$), and the relative humidity was close to saturation at the exit of the test section. The total evaporative loss was computed by obtaining the absolute humidities at the canister inlet and the test section outlet, subtracting these and multiplying by the air mass flow rate, giving the rate at which water evaporated from the drops. Multiplying by the duration of the experiment, the total mass of water lost by evaporation from the fog drops was obtained. For the range of air flow rates considered herein, evaporation was found to be about 10% of the measured mass that left the canister over the duration of the experiment. The evaporative loss was used to correct the values for C, the ratio of liquid flow rate to air flow rate; C is formally defined in the next section.

The setup was operated in two separate modes, the first being the deposition mode, where experiments were run without fog or ultrasonics. In the deposition mode any differences in the upstream and downstream particle counter readings is due to smoke deposition on the tube walls and other surfaces in the flow path, since there are no drops or ultrasonic forces to promote particle loss. The mechanism by which particles were deposited on surface in the flow path may have included charging effects as well as other

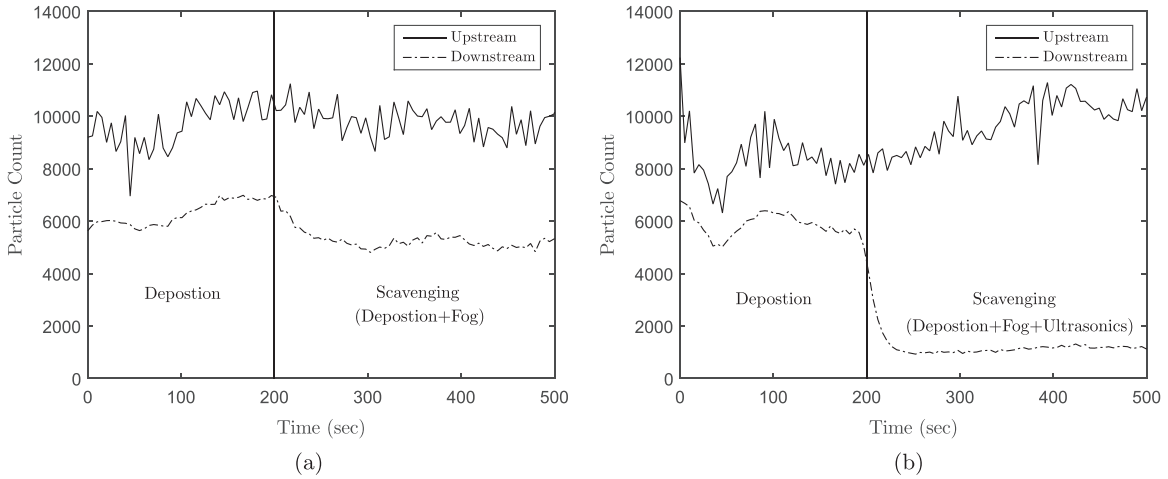

Fig. 10. Time traces showing the two different experiment types performed. An example of an experiment where (a) the scavenging segment is for fog and (b) where the scavenging segment is for fog and ultrasonics.

processes. The second mode was the scavenging mode where fog was used. The difference in upstream and downstream particle counter readings while operating in the scavenging mode was a measure of the combined effect of deposition and particle removal by the fog. The scavenging mode was operated both with and without the ultrasonic standing wave field. Hence, three experimental modes were considered: (i) deposition, (ii) deposition plus fog scavenging, and (iii) deposition plus ultrasonics-enhanced fog scavenging. During an individual experiment, the first 3 minutes were used for the deposition mode, while the remaining 6 minutes were used for one of the fog scavenging modes. For each point in the parameter space, an equal number of runs were performed for the fog scavenging mode and the ultrasonics-enhanced fog scavenging mode. A sample time trace is presented in Fig. 10 for each of the two different experiments. Presented are time traces of particle count for the upstream and downstream particle counters. Fig. 10(a) shows an experiment where the scavenging mode includes just fog, and Fig. 10(b) shows an experiment where ultrasonics and fog were used. The upstream time trace is noisier than the downstream time trace in both plots, which is typical and is presumably due to the relatively short period of time the particles had to mix with the air flow prior to entering the upstream particle counter. To mitigate any error resulting from the noise, ten experimental runs were performed at each point in the parameter space and then averaged, which resulted in a relatively small 95% confidence interval, as is shown in the figures presented in the Results section. The particle counters' coincidence limit was 2 million particles per cubic foot of air, which corresponds to a particle count of 15,000 in Fig. 10. The system was always kept below this upper limit in the experiments presented herein. As was shown previously, independent verification checks of the particle counters showed agreement within 1% of measurements on different counters. As will be shown later in the paper, the measured scavenging in the experiments was on the order of 10–100%, much higher than the deviation between the counters.

Due to the finite distance between the two particle counters (Fig. 6), the particle number density time traces had to be shifted with respect to each other to account for the finite time delay due to convection of the flow from the first particle counter to the second. Time synchronization was done by computing the correlation coefficient for the two time traces while progressively shifting the upstream time trace with respect to the downstream one. The time shift at which the correlation coefficient was maximized was used when computing the scavenging coefficient E. The time shift obtained from the correlation coefficient agreed reasonably well with the time shift obtained by simply dividing the distance between the two particle counters by the average flow velocity in the system, where the average velocity was computed by dividing the volumetric flow rate by the cross sectional area of the resonator. For the flow conditions explored here, these two time delays differed by 17% on average, and the maximum deviation was 24%. Some deviation in the delays computed by these two methods is expected since the flow goes through slight changes in tube diameter and also goes through the fog generator as it travels from the first to the second particle counter, so there is some variation in the flow velocity over the flow path.

The improvement in E due to the presence of ultrasonics was quantified by:

$$I = \frac{E_{wu} - E_{wo}}{E_{wo}} \times 100\% \tag{3}$$

where the subscript *wu* represents experiments with ultrasonics, and *wo* is used for those without ultrasonics. The value of I quantifies the improvement due to the introduction of ultrasonics and fog over fog alone. Deposition is included in the values for both E_{wu} and E_{wo}, and so calculating I according to Eq. (3) eliminates deposition from the numerator. It is, however, present in the denominator, and hence the values of I reported herein are somewhat conservative, and the actual improvement due to ultrasonics is somewhat larger than reported.

House compressed air was used as the flow source for the experiments and the flow rate was metered with a mass flow controller (Aalborg GFC47). The flow propelled the particle-laden air into the fog generation chamber, and then into the test section. The cylindrical resonator is the tube inside the "sealing box" shown in Fig. 6. The tubes upstream and downstream of the cylinder are

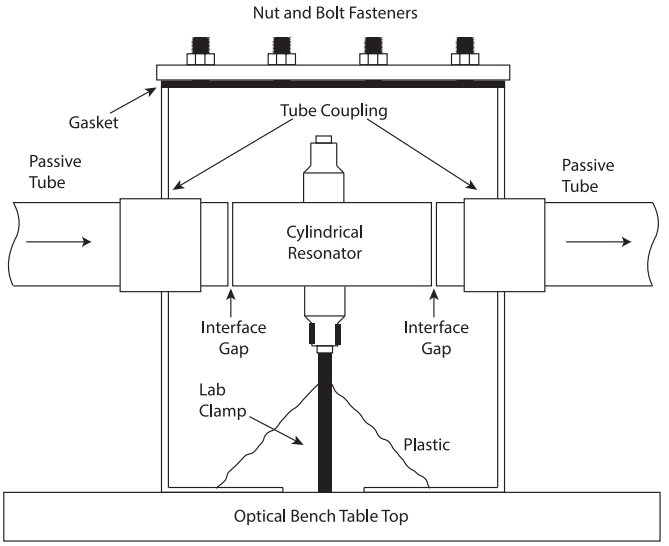

Fig. 11. Schematic illustration of the sealing box used to eliminate direct contact between the cylindrical resonator and the passive tubes, while maintaining flow through all three tubes and minimizing leakage at the passive to active tube interfaces.

referred to as "passive" in the figure because they were not directly driven by the cylindrical resonator. However there was acoustic coupling between the resonator and the passive tubes which was evidenced by fog collecting in nodal rings in the passive tubes. The unforeseen result of rings in the seemingly passive section is an added strength of this approach, as acoustic energy which would otherwise be lost is instead used to lengthen the section where nodes exist, thus increasing the residence time of particles and drops in the field and presumably improving scavenging performance. The passive tubes were made of acrylic, having an inner diameter of 5.08 cm and an outer diameter of 5.7 cm. The length of the upstream passive tube was 60 cm and the downstream tube was 90 cm. A 30 cm segment of the same diameter tubing was used for the vertical segment seen near the exhaust in Fig. 6. Nodal rings were not observed in the vertical segment of the setup.

Connecting the resonator and passive tubes directly was not desirable, as a connection of such a sort damped the vibration of the resonator, weakening the standing wave field. Fig. 11 shows a sealing box which was developed to provide a fluidic seal without the undesirable damping. The box allowed for minimally disturbed flow between the resonator and passive tubes without a direct seal between them. Thus the box provided an air-tight seal with the passive tubes and the resonator, preventing the fog and the particles from leaking at the interfaces. To smooth the transition between the tubes and resonator, the spacing at these interfaces was kept to less than 2 millimeters. The interface gaps were monitored during experiments, and with fog blowing through the system as a visualizer, no fog was observed leaking from the gaps at the interfaces of the cylinder and tubes. It is possible that even with these precautions taken to contain the particles, a small portion of them still may have leaked at the interface into the sealing box. But because the box is sealed, it would then mean that an equivalent amount of fluid would be injected back into the flow at the other interface. Particles behaving in such a manner would have a negative impact on particle scavenging, as particles would be skipping the acoustically active section where it is argued that most of the scavenging is taking place. Therefore, the results presented herein are conservative values of particle scavenging for the setup. The sealing box was made from clear acrylic, having a removable lid for convenience. The cylindrical resonator was mounted to the table top with a lab clamp connected to one of the Langevin transducers.

The cylindrical resonator was excited by the sine-wave output of a function generator (Agilent 33220A) and power amplifier (Krohn-Hite 7500) combination. Because the resonant frequency of the cylinder would drift over the duration of the experimental run, a frequency tracking program was used to keep the device operating as close as possible to the resonant condition. Frequency tracking was done by monitoring the power, P, delivered to the transducers and changing the frequency, f, to keep P at a maximum. The current through the transducers was obtained by measuring the voltage drops across a resistor in series with the transducers. The voltage of the transducers was obtained by simply measuring the drop across all three of the transducers. These two voltages were sampled with an A/D converter (DATAQ DI-158U), and the rms power was calculated as:

$$P = iv(\cos\phi) \tag{4}$$

where v is the rms voltage across the transducers, i is the rms current through the transducers, and ϕ is the phase angle between the current and voltage signals. Though it would reasonably be expected that P would be maximum at $\phi = 0°$, $\phi = 45°$ actually produced maximum P. The above result is not surprising due to the complicated coupling between the resonant frequencies of the Langevins, the air cavity, and the aluminum cylinder. A Matlab program was used to automatically tune f to maintain $\phi = 45°$. Automatic tuning was done by fitting sine waves to the samples obtained from the A/D converter, and then using the calculated ϕ to update f to keep ϕ as close to 45° as possible. The tuning setup was capable of updating f at a rate of 4 times per second, and ϕ was kept at $45 \pm 1°$.

Experiments were performed to test the effect on the scavenging coefficient of both air flow rate, Q, and power, P. The flow rate was varied from 20 to 70 L/min and the power was varied from 0 to 15 W. Results are presented below for the scavenging coefficient

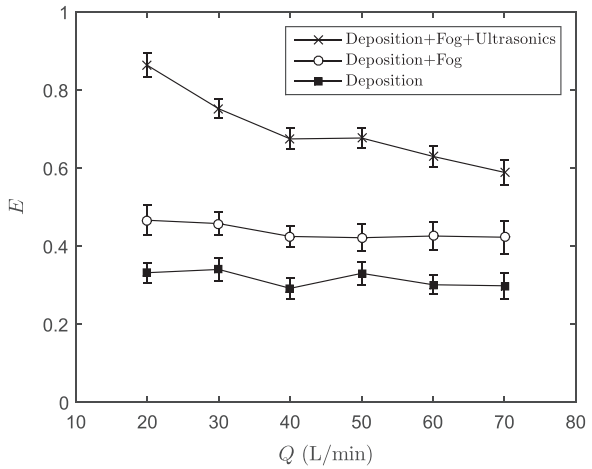

Fig. 12. Scavenging coefficient E versus air flow rate Q for a constant transducer power $P = 2.42 \pm 0.1$ W. The vertical bars are 95% confidence intervals.

and the improvement due to ultrasonics.

3. Results

Fig. 12 is a plot of the scavenging coefficient E versus the air flow rate Q, showing the effect on particle scavenging of deposition, fog, and ultrasonics-enhanced fog. Each data point in Fig. 12 and subsequent plots is an average of ten individual runs, with the vertical bars representing the 95% confidence interval. Modest improvements in the scavenging coefficient are seen with the introduction of fog, and significant improvements are observed with the addition of ultrasonics. At the lowest flow rate plotted in Fig. 12, the scavenging coefficient was greater than 0.8 with ultrasonics present while for the case of deposition alone, $E < 0.4$. Fig. 12 shows that the scavenging coefficient generally decreases with Q for the ultrasonics case, but is relatively constant for the other two cases. An explanation for these two behaviors is presented in the next section.

The improvement in particle removal due to the presence of the ultrasonic standing wave field is better visualized in Fig. 13, which is a plot of the improvement I (Eq. (3)) versus the air flow rate Q, where the maximum I is over 80%. The trend in the figure shows that overall, I decreases with Q, indicating that ultrasonics has less of an improving effect on the scavenging coefficient as the air flow rate increases, suggesting that I is affected by the residence time of particles and drops in the ultrasonic standing wave field.

Ideally, the liquid flow rate would also have been independently varied in the experiments. Unfortunately, with the setup used to generate fog, independently varying the liquid flow rate was not easily achieved. Because the power to the foggers was fixed, so too was the drop generation rate. This fixed fog generation rate might seem to suggest that the flow of drops into the test section was constant, i.e. not a function of air flow rate Q. However, the mass flow of drops was a function of the air flow rate. To facilitate an explanation of the above point, we define the liquid concentration in the air, C:

$$C = \frac{V_l}{Q} \tag{5}$$

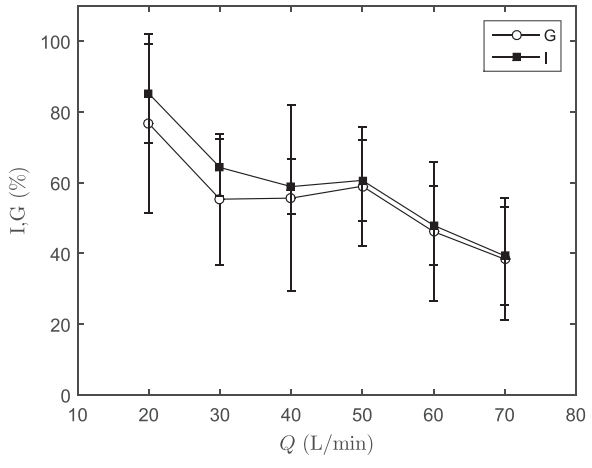

Fig. 13. Improvement I and G (Eq. (6)) plotted against flow rate Q for a constant transducer power $P = 2.42 \pm 0.1$ W. The error bars are 95% confidence intervals.

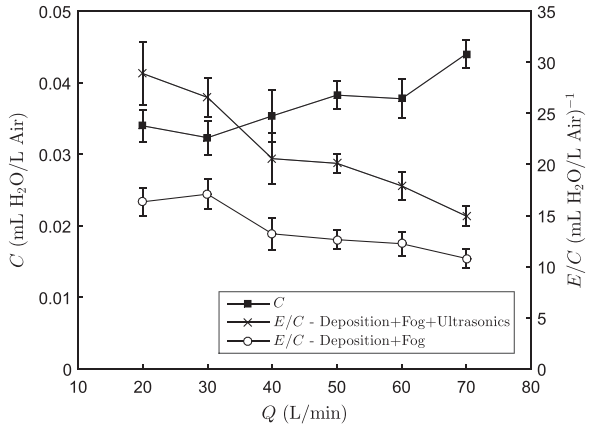

Fig. 14. Plot of C and E/C versus the air flow rate Q. The vertical bars are 95% confidence intervals. The plot of E/C versus Q is for a constant power of $P = 2.42 \pm 0.1$ W.

where V_l is the volumetric flow rate of liquid water measured using the triple beam balance as described in Section 2, above. Note that since the fog drop size distribution was relatively constant from experiment to experiment, C is linearly related to the drop number density in the air flow (number of drops/unit volume of air). Fig. 14 is a plot of C versus the air flow rate Q, showing a slight increase with air flow rate. The reason for the increase is likely due to more fog drops being generated than can be convected away from the canister at low air flow rates. These excess drops likely rise and then fall back into the bulk water of the canister at low flow rates. However, at higher air flow rates, they are convected into the test section, giving the larger value of C at those higher flow rates.

A larger concentration of fog drops C would presumably increase the scavenging of smoke particles. Since C increases with air flow rate, it is possible that the decrease in the scavenging coefficient with air flow rate seen in Fig. 12 would be even larger, had C been independent of the air flow rate. To determine whether C did indeed affect the results, the values of E presented in Fig. 12 are scaled to C and replotted in Fig. 14, giving a plot of E/C versus Q. Unlike Fig. 12, there are only two cases shown, "Deposition + Fog + Ultrasonics" and "Deposition + Fog." Fog is not present during the "Deposition" case and hence is only valid for $C = 0$. From low to high air flow rate, there is an overall decreasing trend in E/C for the two cases, although some adjacent data points are not significantly different from each other. Importantly, the total decrease in E over the full range of air flow rates for the Deposition + Fog + Ultrasonics case shown in Fig. 12 is 29%, while the decrease in E/C over the same range of Q in Fig. 14 is 48%. The trend in the data is expected; the decrease in particle removal with air flow rate is larger when we correct for the fact that the number of drops grows with increasing air flow rate. However, it is also the case that the general trend in particle removal with air flow rate is not qualitatively different in Figs. 12 and 14.

In order to correct the improvement I for variations in C, the variable G is developed where:

$$G = \frac{(E_{wu}/C_{wu}) - (E_{wo}/C_{wo})}{(E_{wo}/C_{wo})} \times 100\% \tag{6}$$

A plot of G versus air flow rate is shown in Fig. 13. While the data points show a decrease with Q, within the 95% confidence intervals there is no real trend indicating that the improvement due to ultrasonics is relatively insensitive to air flow rate when the variation in drop concentration is corrected for. It should be noted that, even when scaled to C, there is still an improvement due to ultrasonics of over 40% at the highest air flow rate tested and 80% at the lowest air flow rate, all using less than 3 Watts of power. The confidence intervals in Fig. 13 are larger than those in previous figures. Although G is calculated from the scavenging coefficient and the concentration C, both of which have fairly small confidence intervals individually, the propagation of uncertainty results in larger 95% confidence intervals for G.

The influence of transducer power P on the scavenging coefficient was investigated for a fixed air flow rate $Q = 50 \pm 1$ L/min. Results are presented in a fashion similar to that above where results for E, I, E/C, and G are presented sequentially. Fig. 15 presents a plot of scavenging coefficient E versus power, revealing an increase in E with transducer power P which appears to be asymptotically approaching unity; at $P = 14.82 \pm 0.92\ W$, $E = 0.93$. Fig. 15 shows a similar trend for I which also increases monotonically with P. The maximum I obtained herein was 120%, which means the ultrasonics provides significant improvement on particle scrubbing over the fog alone at "high" power ($P = 14.82$ W).

The results for the scavenging coefficients shown in Fig. 15 were scaled to C, as was done when the data were plotted against air flow rate. The plot of E/C versus power presented in Fig. 16 is qualitatively similar to that for E versus P in Fig. 15. Also, the correction for variations in C in Fig. 16 has minimal effect on the min to max variation in particle removal with power; the total percent change in E and E/C with P is the same, within the confidence intervals of the data. The trend is expected, since C varies with air flow rate, but the air flow rate is held fixed in Figs. 15 and 16. Finally, the plot of G versus transducer power P in Fig. 15 is virtually the same as that for I versus P. Again, such behavior is expected, as C is not expected to vary in these data where the air flow rate Q is held constant. These plots show that the maximum improvement due to ultrasonics at the highest P tested was ~120%.

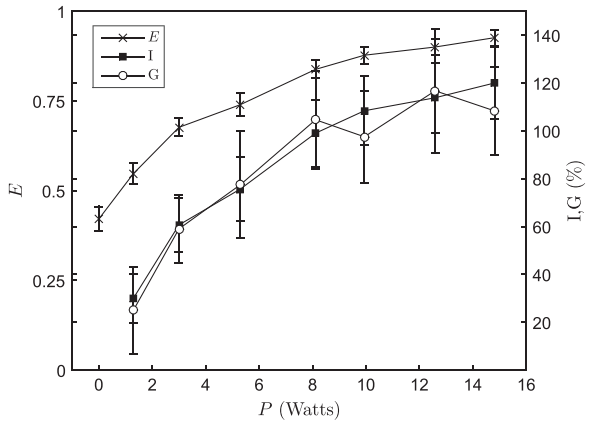

Fig. 15. *E*, *I*, and *G* versus transducer power *P* for a constant air flow rate $Q = 50 \pm 1$ L/min. The vertical bars are 95% confidence intervals.

4. Discussion

The results presented above show significant improvement over the results of Ran et al. (2014) and Ran and Saylor (2015). The highest scavenging coefficient achieved by those researchers was close to 0.2, while for the work presented herein it was 0.93. Also, the flow rate in the previous disk setup was only 12 L/min while in the present work, significant scavenging coefficients were obtained at flow rates as large as 70 L/min. The above results also show that the scavenging coefficient decreases with air flow rate, and increases with power, both of which were expected. Decreasing the air flow rate increases the residence time in the ultrasonic standing wave field and in the passive tubes, which gives more time for drops and particles to combine. Increasing power increases the strength of the field which allows particles and drops to be compressed into a smaller volume in the nodes, thus leading to more combinations between them. A detailed discussion is now presented of potential mechanisms that can explain the magnitude of the scavenging coefficient for the various conditions explored.

A two step process is used here to explain the removal of particles by drops in the presence of an ultrasonic standing wave field. The process begins with an increase in the number density of drops and particles as they are pushed into the nodes of the standing wave field. Then, diffusive motion of particles to drops is used to explain the ultimate removal of particles. For simplicity, particle scavenging is modeled as a sequential two step process, though in reality both processes will occur simultaneously and may also be coupled to each other, a process which is not captured in the presented model. In the first step, the equation for the acoustic radiation force is used to obtain estimates for the increase in the particle and the drop number density at the nodes of the standing wave field. The second step is a model of particle removal (at a now increased number density for both particles and drops) via diffusion of particles toward drops. As will be shown, the two step model works well at high transducer power, but not for low power.

To model the increase in number density of particles and drops in the nodes, the viscous model of the acoustic radiation force due to Settnes and Bruus (2012) is used with the cylindrical acoustic field theory of Barmatz and Collas (1985), F_{ar}, giving:

$$F_{ar} = \frac{\widetilde{F}(\pi d^3 \rho_a U_a^2 k_\lambda)}{8} \tag{7}$$

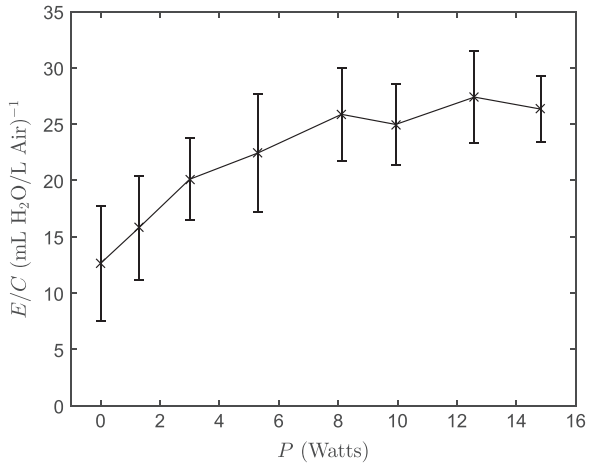

Fig. 16. *E*/*C* versus *P* for a constant $Q = 50 \pm 1$ L/min. The vertical bars are 95% confidence intervals.

where

$$\widetilde{F} = \left(\left[\left(\frac{2f_1}{3}\right) + \left(\frac{f_2}{2}\right)\right]J_0(\chi) - \left(\frac{f_2}{2}\right)J_2(\chi)\right)J_1(\chi) \tag{8}$$

$$f_1 = 1 - \frac{\rho_a c_a^2}{\rho c^2} \tag{9}$$

$$f_2(\widetilde{\rho}, \widetilde{\delta}) = \Re\left[\frac{2[1 - \gamma(\widetilde{\delta})](\widetilde{\rho} - 1)}{2\widetilde{\rho} + 1 - 3\gamma(\widetilde{\delta})}\right], \tag{10}$$

where

$$\delta = \sqrt{\frac{2\nu}{\omega}} \tag{11}$$

$$\widetilde{\rho} = \frac{\rho}{\rho_a}, \tag{12}$$

$$\gamma(\widetilde{\delta}) = -(3/2)[1 + i(1 + \widetilde{\delta})]\widetilde{\delta} \tag{13}$$

and

$$\widetilde{\delta} = \frac{\delta}{d/2} \tag{14}$$

where d is the diameter of the drop or particle, U_a is the maximum acoustic particle velocity, k_λ is the acoustic wave number, J_B is the Bessel function of order B, ρ_a and c_a are the air density and air sound speed, respectively, ρ and c are the drop or particle density and sound speed, respectively, ν is the kinematic viscosity of the air, ω is the angular frequency of the acoustic wave, and δ is the acoustic boundary layer thickness. In order to evaluate Eqs. (7)–(14), a value for U_a, the maximum acoustic particle velocity is required. The value for the maximum acoustic particle velocity was obtained by levitating a millimeter diameter drop in the cylinder and slowly lowering P until the drop fell. Then, by setting the weight of the fallen drop equal to F_{ar}, U_a was solved for, given that it was the only unknown in the equation for F_{ar}. The described approach gave $U_a = 10$ m/s. The minimum P to levitate was found to be ~1 W, and for evaluating higher powers, F_{ar} was assumed to scale linearly with power.

Using the above theory for the acoustic radiation force, the motion of drops and particles to the nodes of the standing wave field was calculated by integrating $F_{ar} - F_d$ over the residence time in the cylindrical resonator, where F_d is the Stokes drag on the particle:

$$F_d = 3\pi\mu_a u_r d \tag{15}$$

where u_r is the velocity of the particle or drop in the radial direction towards the node. A volumetric flow rate $Q = 50$ L/min, which lies between the minimum and maximum flow rates considered here, was chosen as a test case and corresponds to residence times of 0.3 seconds in the cylindrical resonator and 4 seconds in the test section respectively. Although particles and drops enter the test section evenly distributed across the tube cross section, for simplicity it was assumed that they all originated in the antinodes and that their number density would only increase due to their motion toward the nodes. Employing these assumptions provides a conservative estimate, since there are many particles and drops closer to the node at the test section entrance and these would move to the nodes much sooner than the described analysis implies. The distance a drop and/or particle moved toward the node in the residence time of the resonator was used to obtain an estimate of the localized number density of particles and drops at the nodes. For example, if the particles moved halfway to the node during the residence time of the resonator, the number density was increased by a factor of two.

Once an increase in the number density of drops and particles is obtained, particle loss is computed using the following equations which predict collisions between particles and drops assuming that the particles diffuse toward the drops via Brownian motion and that the drops are sufficiently large that they do not move due to Brownian motion at all. Given that the drops were several microns in diameter and the smoke particles were submicron in size, the assumption of negligible Brownian motion is imperfect, though reasonable for an order of magnitude analysis. Under these conditions,

$$E = 1 - e^{-\Lambda_c t} \tag{16}$$

where t is time and Λ_c is the fractional particle removal rate (Pruppacher & Klett, 1978):

$$\Lambda_c = 2\pi\mathcal{D}\int_0^\infty d_d N(d_d) d(d_d) \tag{17}$$

where $N(d_d)$ is the size distribution of fog drops and $\mathcal{D}$ is the diffusion coefficient of the particles:

$$\mathcal{D} = \frac{k_b T C_c}{3\pi\mu_a d_p} \tag{18}$$

where k_b is Boltzmann's constant, T is temperature of the air, μ_a is the dynamic viscosity of the air, d_p is the particle diameter, and C_C

is the Cunningham correction factor:

$$C_c = 1 + \frac{2.52\alpha}{d_p} \tag{19}$$

where α is the mean free path of air. These equations are used to obtain predictions for E at a small and large value of P explored here: $P = 2.24$ W and $P = 12.59$ W. For $P = 2.24$ W, integrating $F_{ar} - F_d$ for both drops and particles across the residence time of the cylindrical resonator showed their motion to be very similar. The motion corresponded to an order of magnitude increase in the drop and particle number densities at the nodes, compared to the case without any ultrasonics. Evaluating Eq. (16) for $P = 2.24$ W with an order of magnitude increase in the drop number density for the total residence time of the test section gives $E = 0.012$, which deviates significantly from the experimentally obtained value of $E = 0.51$. Repeating the process for $P = 12.59$ W shows that particles and drops will have moved within 1 μm of the nodes, corresponding to an increase in number density of ~7000. Once drops have moved within a diameter of each other, 5 μm, no further increases can be obtained since the drops will be touching. Hence, instead of increasing the drop number density by a factor of 7000, we simply estimate that the drop number density has increased by three orders of magnitude which accurately represents the increase in number density when the drops just barely touch. Evaluating Eq. (16) for $P = 12.59$ W gives $E = 0.70$, which is comparable to the experimental value of $E = 0.89$. The above analysis suggests that the increase in the number density of drops and particles by F_{ar}, followed by diffusive scavenging predicted by Eqs. (16) through (19) explains the values of scavenging coefficient observed for the high power ultrasonics case within an order of magnitude. As previously discussed, the scavenging model for the high power case does not account for the simultaneous nature of the processes, which may produce a coupling which could explain the discrepancy seen herein. At low power, the theory does not predict the scavenging to within an order of magnitude and an alternative explanation is necessary.

Particle removal for $P \to 0$ can be explained in part by gravitational settling of fog drops. The settling velocity is much higher for fog drops than it is for the submicron particles, thus generating a relative velocity between the two. Gravitational settling allows for drops to impact particles and remove them from the system. For the situation of purely gravitational settling leading to particle-drop collisions, the scavenging coefficient is:

$$E = 1 - e^{-\Lambda_p t} \tag{20}$$

where the fractional particle removal rate, Λ_p, is (Wang, Zhang, & Moran, 2010):

$$\Lambda_p(d_p) = \int_0^\infty \frac{\pi}{4}(d_p + d_d)^2 (V(d_d) - v(d_p)) Z(d_p, d_d) N(d_d) d(d_d) \tag{21}$$

where $V(d_d)$ and $v(d_p)$ are the terminal velocities of the drop and particle respectively, $Z(d_p, d_d)$ is the drop-particle collection efficiency (Wang et al., 2010):

$$Z(d_p, d_d) = \frac{4}{ReSc}[1 + 0.4Re^{1/2}Sc^{1/3} + 0.16Re^{1/2}Sc^{1/2}] + 4\frac{d_p}{d_d}\left[\frac{\mu_a}{\mu_d} + (1 + 2Re^{1/2})\frac{d_p}{d_d}\right] + \left(\frac{St - St^*}{St - St^* + 2/3}\right)^{3/2} \tag{22}$$

where

$$V(d_d) = \frac{d_d^2(\rho_d - \rho_a)gC_c}{18\mu_a}, \quad Re = \frac{d_d V(d_d)\rho_a}{2\mu_a}, \quad Sc = \frac{\mu_a}{\rho_a \mathcal{D}} \tag{23}$$

and

$$St = \frac{2\tau(V(d_d) - v(d_p))}{d_d}, \quad \tau = \frac{(\rho_p - \rho_a)d_p^2 C_c}{18\mu_a}, \quad St^* = \frac{1.2 + \frac{1}{12}\ln(1 + Re)}{1 + \ln(1 + Re)} \tag{24}$$

where Re is the drop Reynolds number, Sc is the Schmidt number for the particles, St is the Stokes number for the particles, ρ_d is the drop density, ρ_a is the air density, g is the acceleration due to gravity, τ is the particle relaxation parameter, and μ_d is the dynamic viscosity of the drop fluid. Using the DSD in Fig. 9 and C from Fig. 14, Eqs. (20)–(24) were integrated over the residence time of the test section. The previously described process was done for $d_p = 0.5$ μm, corresponding to the most common particle diameter (Fig. 8). Such a process gave $E = 0.15$ for $Q = 50$ L/min which compares well with the experimentally obtained value of $E = 0.42$ for $P = 0$, which improves on the explanation presented above, suggesting that at low power, scavenging by the falling fog drops impacting the particles dominates over the effect of the ultrasonics. However, the predicted value still falls short of the measured one, necessitating further explanation.

One possible explanation for the discrepancy as $P \to 0$ is particle loss due to deposition. Due to the constancy of E due to deposition with air flow rate (Fig. 12), it is possible that particle deposition is primarily occurring due to diffusion in the second particle counter sampling section (tubing and diffusion dryers leading to the downstream particle counter shown in Fig. 6). The flow rate through the sampling section is driven by the downstream particle counter pump, which pulls in air at a constant rate of 3 L/min; hence air flow rate has no impact on residence time and, therefore, on deposition. The residence time of particles from the time they leave the exhaust tube to the time they enter the particle counter is ~30 seconds. Therefore, particles have a significant amount of time to move by diffusion and impact on a wall or on the diffusion dryer media. The diffusion length scale, $\mathcal{L}$, is (Hinds, 1982):

$$\mathcal{L} = \sqrt{2\mathcal{D}t} \tag{25}$$

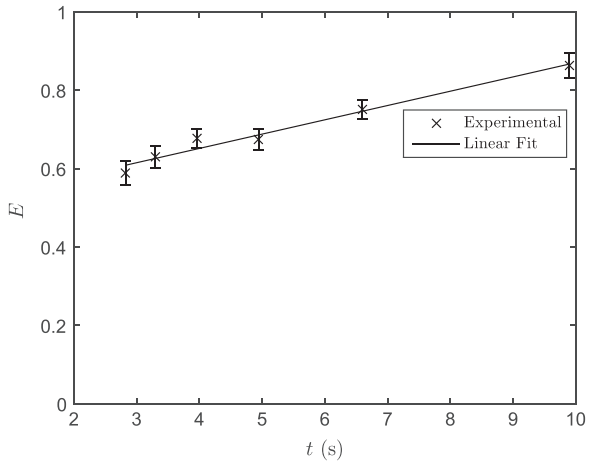

Fig. 17. Plot of scavenging coefficient E versus residence time, t, for the deposition + fog + ultrasonics case; $P = 2.42 \pm 0.1$ W.

where $\mathcal{D}$ is the diffusion coefficient of the particles (Eq. (18)). Evaluation of Eq. (18) for 0.5 μm particles in room temperature air gives $\mathcal{D} = 6.31 \times 10^{-7}$ cm^2/sec, which gives $\mathcal{L} = \sim 60$ μm for $t = 30$ sec. Therefore, particles within ~60 μm of the tube at the beginning of the sampling segment could potentially deposit on the wall during the flow towards the particle counter. The tubing in the sampling section had an average diameter of about 1 cm, therefore, the fraction of particles that are within 60 μm of the tube wall at the beginning of the segment is 0.02. Adding 0.02 to E predicted for $P = 0$, $E = 0.15$, gives a total $E = 0.17$ which is only somewhat closer to the experimentally obtained value of 0.42. Had the flow fallen into the turbulent regime, turbulent flow effects could aid in the motion of particles to drops. However, at the highest air flow rate, the Reynolds number was 1840, signifying laminar or, at worst, mildly transitional flow, and therefore flow oscillations are unlikely to have had any significant effect on scavenging.

To summarize, the particle loss in the system was modeled as a two step process, with different mechanisms at high and low power. At high power the results are explained by particle diffusion alone, enhanced by the increase in number density caused by ultrasonics. However, as $P \rightarrow 0$ the strength of the standing wave field decreases, and the gravitational settling of drops gives a better estimate of the particle loss. Also playing a small role in the $P \rightarrow 0$ case is the removal of particles by deposition onto areas of the experimental setup. In actuality, these processes are all happening simultaneously, and a more sophisticated analysis would simulate these effects in parallel.

An explanation for the trends in scavenging coefficient with air flow rate and power is now presented. For the ultrasonics case, the trend with air flow rate can be easily explained by residence time. A plot of scavenging coefficient versus the residence time, t is presented in Fig. 17 along with a linear fit, showing fairly good agreement, though there is one point for which the fit does not fall within the 95% confidence interval. The linear increase in scavenging coefficient with residence time suggests that the decrease in scavenging coefficient with air flow rate is simply due to (i) less time for particles to be brought closer together by the ultrasonic standing wave field, and (ii) less time for particles to diffuse toward drops. The above explains the trend with air flow rate for the ultrasonics case, but does not explain why for the non-ultrasonics case the scavenging coefficients are relatively constant with air flow rate. Such constancy would not be expected if residence time dictated scavenging coefficient for the non-ultrasonics case.

One possible explanation for the constant trend of scavenging coefficient with air flow rate for the case with fog but no ultrasonics comes from an error which can occur by predicting particle loss with the drop settling theory previously presented. In that analysis it was assumed that there was an unending source of fog. That is, as the fog falls downward, whatever is depleted from the top of the

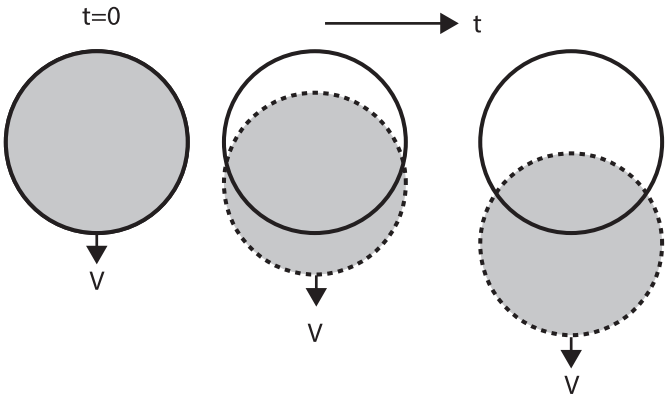

Fig. 18. Growth in blank space in tube cross section with increasing t as fog falls downward. Fog is depicted in the dotted circle, falling at the drop settling velocity defined in Eq. (23).

tube as it falls downward, is somehow replaced. Of course in the experimental setup, fog is not replaced from the tops of the tubes. At the beginning of the test section, the entire cross section is filled with fog and as the fog falls, a blank space without fog is developed at the top of the tube cross section. The settling process is shown schematically in Fig. 18 and was observed experimentally by looking down the axis during experimental operation. Because the falling drops will not remove all of the particles, there will still be particles left in the blank space which the fog vacates. The error introduced by the blank space could then explain why the trend with scavenging coefficient is constant with air flow rate for the case of fog without ultrasonics. Longer residence times allow more time for drops to fall and collide with particles, but also more time for a larger blank space to develop in the top of the tubes, thus less accurate predictions of the scavenging coefficient. Because both the particle loss and blank space are linearly related to the residence time, these trends may offset each other, giving a plausible reason for the constancy of the scavenging coefficient with air flow rate seen experimentally for the case without ultrasonics.

Finally, the trend of the scavenging coefficient with power is now discussed. Fig. 15 shows that the scavenging coefficient is continuously increasing for the range of powers tested. The trend shows an asymptotic increase towards the maximum of unity. Assuming that the acoustic power scales with transducer power, increasing power correspondingly increases the strength of the standing wave field. As such, particles and drops should be compressed into smaller regions in the nodes, allowing for more diffusive combinations during the same residence time, and leading to higher scavenging coefficients. Since the upper bound on the scavenging coefficient is unity, that the data should asymptotically approach the limit of $E = 1.0$, as expected.

5. Conclusion

An ultrasonic standing wave field developed in a cylindrical resonator operating at a nominal frequency of 29 kHz was used to scavenge micron-scale particles from an air flow. The effect of air flow rate and applied power were investigated. For a given power, the scavenging coefficient decreased with air flow rate. For a given air flow rate, the scavenging coefficient increased with power. The results obtained herein produced results improving upon those due to Ran et al. (2014) and Ran and Saylor (2015). The largest scavenging coefficient was 0.93 and was obtained using less than 20 Watts of power. The flow rate capacity of the device was higher than that of previous researchers.

Acknowledgments

This work was supported by the National Science Foundation under Grant No. 1336632.

References

Barmatz, M., & Collas, P. (1985). Acoustic radiation potential on a sphere in plane, cylindrical, and spherical standing wave fields. *Journal of Acoustics Society of America*, *77*, 928–945.
Cohen, A. J. (2000). Outdoor air pollution and lung cancer. *Environmental Health Perspectives*, *108*, 743–750.
Dietrich, G. (1963). *General oceanography* New York, NY: John Wiley & Sons.
Fann, N., Lamson, A. D., Anenberg, S. C., Wesson, K., Risley, D., & Hubbell, B. J. (2012). Estimating the national public health burden associated with exposure toambient PM2.5 and ozone. *Risk Analysis*, *32*(1), 81–95.
Faraday, M. (1831). On the forms and states assumed by fluids in contact with vibrating elastic surfaces. *Philosophical Transactions of the Royal Society of London*, *121*, 319–340.
Heyder, J., Gebhart, J., Rudolf, G., Schiller, C. F., & Stahlhofen, W. (1986). Deposition of particles in the human respiratory tract in the size range 0.005–15 μm. *Journal of Aerosol Science*, *17*(5), 811–825.
Hinds, W. C. (1982). *Aerosol technology: properties, behavior, and measurement of airborne particles* New York, NY: Wiley-Interscience.
Johnson, R. L. (2004). Relative effects of air pollution on lungs and heart. *Circulation*, *109*, 5–7.
Kaduchak, G., Sinha, D. N., & Lizon, D. C. (2002). Novel cylindrical air-coupled acoustic levitation/concentration devices. *Review of Scientific Instruments*, *73*, 1332–1336.
Kim, H. T., Jung, C. H., Oh, S. N., & Lee, K. W. (2001). Particle removal efficiency of gravitational wet scrubber considering diffusion, interception, and impaction. *Environmental Engineering Science*, *18*(2), 125–136.
Kim, S. H., & Lee, K. W. (1999). Experimental study of electrostatic precipitator performance and comparison with existing theoretical prediction models. *Journal of Electrostatics*, *48*(1), 3–25.
Lang, R. J. (1962). Ultrasonic atomization of liquids. *Journal of Acoustics Society of America*, *34*, 6–8.
Lee, K., & Liu, B. Y. H. (1980). On the minimum efficiency and the most penetrating particle size for fibrous filters. *Journal of the Air Pollution Control Association*, *30*(4), 377–381.
Liu, B. Y. H. (1975). *Fine particles: Aerosol generation, measurement sampling, and analysis* New York: Academic Press Inc.
Marple, V. A., & Willeke, K. (1976). Impactor design. *Atmospheric Environment*, *10*, 891–896.
Marple, V. A., Liu, B. Y. H., & Whitby, K. T. (1974). Fluid mechanics of the laminar flow aerosol impactor. *Journal of Aerosol Science*, *5*(1), 1–16.
McCubbin, T. K. (1953). The particle size distribution in fog produced by ultrasonic radiation. *Journal of Acoustics Society of America*, *25*, 1013–1014.
Peskin, J. L., & Raco, R. J. (1963). Ultrasonic atomization of liquids. *Journal of Acoustics Society of America*, *35*, 1378–1381.
Pope, C. A., Thun, M. J., Namboodiri, M. M., Dockery, D. W., Evans, J. S., Speizer, F. E., et al. (1995). Particulate air pollution as a predictor of mortality in a prospective study of U.S. adults. *American Journal of Respiratory and Critical Care Medicine*, *151*, 669–674.
Ran, W., & Saylor, J. R. (2015). A mechanistic explanation of the increase in particle scavenging in the ultrasonic scrubber. *Journal of Aerosol Science*, *87*, 88–101.
Pruppacher, H., & Klett, J. (1978). *Microphysics of clouds and precipitation* Dordrecht: Reidel Publishing Company.
Ran, W., Saylor, J. R., & Holt, R. G. (2014). Improved particle scavenging by a combination of ultrasonics and water sprays. *Journal of Aerosol Science*, *67*, 104–118.
Rasband, W.S. (1997–2009). ImageJ. *National Institutes of Health*, Bethesda, Maryland, USA.
Schwartz, J., Laden, F., & Zanobetti, A. (2002). The concentration-response relation between PM2.5 and daily deaths. *Environmental Health Perspectives*, *110*(10), 1025–1029.
Seaton, A., MacNee, W., Donaldson, K., & Godden, D. (1995). Particulate air pollution and acute health effects. *The Lancet*, *345*, 176–178.
Settnes, M., & Bruus, H. (2012). Forces acting on a small particle in an acoustical field in a viscous fluid. *Physical Review E*, *85*(1), 016327.
Tucker, W. G. (2000). An overview of PM2.5 sources and control strategies *Fuel Processing Technology 65-66*, 379–392.

Wang, X., Zhang, L., & Moran, M. D. (2010). Uncertainty assessment of current size-resolved parameterizations for below-cloud particle scavenging by rain. *Atmospheric Chemistry and Physics*, *10*, 5685–5705.

Wood, R. W., & Loomis, A. L. (1927). The physical and biological effects of high-frequency sound-waves of great intensity. *Philosophical Magazine*, *4*, 417–436.

Yang, J., Hwang, H., Youngmin, B., Moojoon, K. & K.H. (2012). Trapping of microparticles in the cylindrical standing 524 wave field. *Proceedings of symposium of ultrasonic electronics* (Vol. 33, pp. 281–282).